Research Square

Preprints are preliminary reports that have not undergone peer review.
They should not be considered conclusive, used to inform clinical practice,
or referenced by the media as validated information.

Design and Recombinant Production of Proline-rich Antimicrobial Peptide 385P

Zülal Kesmen

zkesmen@erciyes.edu.tr

Erciyes University

Melike Canpolat

Erciyes University

Dilara Herdem

Erciyes University

Research Article

Keywords: Proline-rich antimicrobial peptides, Peptide design, Conserved motifs, Recombinant production, Antibiofilm activity, Protease stability

Posted Date: November 4th, 2026

DOI: https://doi.org/10.21203/rs.3.rs-11365499/v1

License: This work is licensed under a Creative Commons Attribution 4.0 International License.
Read Full License

Additional Declarations: No competing interests reported.

Title: Design and Recombinant Production of Proline-rich Antimicrobial Peptide 385P

Authors: Zülal Kesmen Department of Food Engineering, Faculty of Engineering, Erciyes University, 38039 Kayseri, Türkiye: zkesmen@erciyes.edu.tr

Melike Canpolat Engineering Faculty, Department of Food Engineering, Erciyes University, Kayseri, Türkiye, melikeccanpolat@gmail.com

Dilara Herdem Engineering Faculty, Department of Food Engineering, Erciyes University, Kayseri, Türkiye, d_herdem@hotmail.com

*Corresponding author: zkesmen@erciyes.edu.tr

Design and Recombinant Production of Proline-rich Antimicrobial Peptide 385P

Zülal Kesmen[1,] * (https://orcid.org/0000-0002-4505-6871)

Melike Canpolat[1] (https://orcid.org/0000-0003-0345-465X)

Dilara Herdem[1] (https://orcid.org/0000-0001-5006-5708)

1 Engineering Faculty, Department of Food Engineering, Erciyes University, Kayseri, Türkiye

* Correspondence: Zülal Kesmen, Engineering Faculty, Department of Food Engineering, Erciyes University, Kayseri, Türkiye. Email address: zkesmen@erciyes.edu.tr

ABSTRACT

The rapid emergence of antimicrobial resistance has increased the search for alternative agents with novel mechanisms of action. Here, we established an end-to-end framework for the rational development of proline-rich antimicrobial peptides (PrAMPs), integrating computational motif discovery, peptide design, recombinant

production, and biological characterization. Conserved motifs from highly active PrAMPs were identified and ranked using MEME and rationally assembled to generate the 36-amino acid peptide 385P. A C-terminal hexahistidine-tagged construct (r385P) was successfully produced in *Pichia pastoris* GS115 and confirmed by SDS-PAGE, Western blotting, and His-tag ELISA. r385P exhibited broad-spectrum antimicrobial activity, with MICs of 4–32 μg/mL against Gram-negative bacteria, 2–32 μg/mL against Gram-positive bacteria, and 64 μg/mL against *Candida albicans* and *Candida glabrata*, with the highest antibacterial activity against *Listeria monocytogenes* and *Acinetobacter baumannii*. r385P exhibited strong antibiofilm activity, achieving 83.83% inhibition against *Escherichia coli* O157:H7 at MIC/2 and complete inhibition against *Staphylococcus aureus* at MIC. FICI assays revealed antibiotic- and species-dependent interactions, including synergy with kanamycin against *Klebsiella pneumoniae* (FICI = 0.375) and consistent additive interactions with tetracycline. r385P retained full antimicrobial activity after exposure to 50–200 mM NaCl and 1–4 h of trypsin treatment, while MICs increased two- and four-fold following exposure to 65 and 95 °C, respectively. Hemolysis remained below 4% at 256 μg/mL, while MRC-5 cell viability was 71% at 320 μg/mL. Collectively, these findings demonstrate the potential of conserved-motif assembly as a practical strategy for developing functionally robust PrAMP candidates.

Keywords: Proline-rich antimicrobial peptides; Peptide design; Conserved motifs; Recombinant production; Antibiofilm activity; Protease stability

1. INTRODUCTION

The rapid global spread of antibiotic-resistant pathogens has significantly reduced the effectiveness of conventional therapeutics, highlighting the urgent need for novel antimicrobial agents. Antimicrobial peptides (AMPs), which serve as the first line of defense against pathogenic microorganisms in many organisms, have emerged as promising alternatives to antibiotics [1]. Proline-rich antimicrobial peptides (PrAMPs) are a class of host defense peptides characterized by a high proportion (≥25%) of proline residue [2,3]. The cyclic pyrrolidine side chain of proline residues restricts backbone conformational flexibility and introduces local rigidity. This unique structural feature profoundly influences the molecular behavior and biological activity of PrAMPs [4]. However, rather than promoting rigid α-helical architectures, a high proline content often favors disordered or type II polyproline (PPII)-like conformations [5]. This structural feature facilitates molecular recognition and conformational adaptability, enabling PrAMPs to interact effectively with intracellular targets, including ribosomes and chaperone proteins such as DnaK [6,7]. Following their uptake into bacterial cells via specific

transporters such as SbmA, YgdD, and MdtM, PrAMPs interact with these intracellular targets, thereby killing bacteria through non-lytic mechanisms, unlike conventional antimicrobial peptides [8,9]. One of the primary intracellular targets of PrAMPs is the bacterial 70S ribosome. Recent studies have demonstrated that PrAMPs inhibit bacterial protein synthesis by interacting with the ribosome [10,11]. Different classes of PrAMPs inhibit protein biosynthesis by targeting distinct ribosomal sites. Oncocin-type peptides inhibit protein synthesis by blocking the ribosomal exit tunnel during translation initiation and early elongation, whereas apidaecin-type peptides inhibit ribosome recycling by trapping release factors (RF1/RF2) on the ribosome during translation termination [12,13]. In addition to ribosomal inhibition, certain PrAMPs bind to the C-terminal helix of bacterial DnaK, thereby disrupting chaperone-assisted protein folding and stress responses [14–17]. These distinct mechanisms of action may limit resistance development and enhance the antimicrobial efficacy of PrAMPs against multidrug-resistant (MDR) bacteria [18]. PrAMPs can also synergize with conventional antibiotics, potentially improving efficacy while reducing the required antibiotic doses [19–21]. For example, A3-APO showed synergistic effects with colistin against K. pneumoniae and A. baumannii, likely through complementary mechanisms of action targeting DnaK-mediated protein folding and bacterial membranes [19]. A3-APO has also been reported to enhance the activity of several conventional antibiotics against MDR strains through the inactivation of resistance enzymes [22]. Collectively, these findings support PrAMP–antibiotic combinations as a potential strategy for combating MDR bacteria.

Despite their therapeutic potential, natural PrAMPs often exhibit a relatively narrow antibacterial spectrum, with activity restricted to specific bacterial species. Rational optimization of natural PrAMP sequences can overcome this limitation by generating synthetic derivatives with enhanced potency and broader activity through improved interactions with intracellular targets such as the ribosome and DnaK [23]. Motif-based approaches in PrAMPs design represent an important strategy for enhancing biological activity and specificity. These methods utilize conserved short motifs frequently found in natural PrAMPs as a starting point for designing synthetic derivatives. Conserved motifs in natural PrAMPs play key roles in antimicrobial activity by mediating cellular uptake and interactions with intracellular targets [8]. For example, the N-terminal RRIR motif of Bac7 is associated with membrane interaction and cellular uptake, whereas PIRXP repeats contribute to ribosome binding [24,25,26]. Similarly, the conserved proline-rich motifs YLPRP and YSPRP in pyrrhocoricin and drosocin, respectively, are involved in DnaK binding [27,28]. These findings suggest that combining functionally relevant motifs from natural PrAMPs may provide a rational strategy for designing synthetic peptides with enhanced antimicrobial activity.

Direct isolation and purification of PrAMPs from natural sources are highly labor-intensive and costly and may pose potential threats to wildlife. Although solid-phase peptide synthesis (SPPS) is widely used for peptide production [29], the backbone rigidity associated with high proline content can complicate peptide chain elongation. The high proline content can also promote chain folding, potentially masking reactive sites, hindering coupling reactions, and leading to the formation of unwanted by-products. Therefore, recombinant expression approaches offer a more convenient and efficient alternative for producing such peptides. Recombinant DNA technology enables the cost-effective and scalable production of standardized-quality AMPs using microorganisms such as bacteria and yeasts that can be readily genetically manipulated [29]. Among available expression systems, *Pichia pastoris* is particularly attractive due to its high expression capacity, lack of endotoxins, ability to perform post-translational modifications, and efficient secretion, which can facilitate downstream purification [30,31].

Despite their distinctive intracellular mechanisms, low cytotoxicity, and resistance to proteolytic degradation, the therapeutic potential of PrAMPs can be limited by their relatively narrow antimicrobial spectrum. To address this limitation, this study aimed to develop a rational design strategy for producing a PrAMP with enhanced potency and broad-spectrum activity against drug-resistant microorganisms. The study also aimed to express the designed PrAMP recombinantly in *Pichia pastoris*, a suitable platform for the production of *de novo*-designed antimicrobial peptides.

2. MATERIAL AND METHODS

2.1. Design of 385P peptide

The design strategy for the 385P peptide was based on the assembly of conserved structural motifs derived from PrAMPs exhibiting high antimicrobial activity. For this, a dataset was generated by selecting peptides from the following members of PRP families in the Database of Antimicrobial Activity and Structure of Peptides (DBAASP): Abaecin (*Apis mellifera*), Arasin, Bac5 (1–23), Bac7 (1–35), Drosocin, Formaecin, Metchnikowin, Oncocin, PR-39, Pyrrhocoricin, Tur1A, Tur1B, and Myticalin. Only peptides exhibiting MIC values <50 μg/mL against *E. coli* were considered active and included in the dataset, whereas peptides with MIC values >50 μg/mL were excluded. Additionally, the peptides shorter than < 9 amino acids, exhibiting over 90% similarity and containing unusual amino acids, were eliminated from the dataset. The remaining peptides were analyzed using the MEME Suite motif discovery tool (https://meme-suite.org/meme/tools/meme version 5.5.9) by selecting the motif length set to between 4 and 9 amino acids. The obtained motifs were ranked for statistical significance, and the 5 motifs with the smallest E-value were selected for use in the design. Candidate peptides were constructed by

assembling four-motif combinations from the five top-scoring motifs (with the lowest E values) identified via MEME analysis. The physicochemical properties of all candidate peptides were predicted using the HeliQuest program (https://heliquest.ipmc.cnrs.fr/cgi-bin/ComputParams.py). Peptides other than those with a net charge between +2 and +7 and a hydrophobicity value between 0.30 and 0.50 were excluded from the data set.

The antimicrobial activities of the remaining peptides were estimated using $CAMP_{R3}$ (http://www.camp3.bicnirrh.res.in/), and hemolytic potentials were estimated using HemoPI2 (https://webs.iiitd.edu.in/raghava/hemopi2/prediction.html). The peptide with the highest antimicrobial activity and the lowest hemolytic activity scores was selected for heterologous production by the recombinant method. The 385P peptide comprised five motifs, each containing four to nine amino acid residues derived from pyrrhocoricin, myticalin, and drosocin, with an additional N-terminal glycine residue introduced to improve peptide stability (Fig. 1).

2.2. Prediction of physicochemical properties of 385P

The physicochemical properties of the peptides were evaluated using various web-based tools. Molecular weight, net charge, and isoelectric point (pI) were calculated using the Peptide Property Calculator (https://pepcalc.com/). Hydrophobicity values were determined using HeliQuest (https://heliquest.ipmc.cnrs.fr/cgi-bin). Hemolytic potential and toxicity were predicted using HemoPI (https://webs.iiitd.edu.in/raghava/hemopi/index.php) and ToxinPred respectively, (https://webs.iiitd.edu.in/raghava/toxinpred/algo.php). The antimicrobial activity of the peptides was predicted using CAMPR3 (http://www.camp.bicnirrh.res.in/).

2.3. Construction of the expression vector and transformation into *P. pastoris*

The pPICZαA vector (Thermo Fisher Scientific, USA) was used for heterologous expression of 385P. The 385P coding sequence was reverse-translated using the EMBOSS Backtranseq tool (https://www.ebi.ac.uk/Tools/st/emboss_backtranseq/), and codon optimization was performed for *P. pastoris* using ATGme (http://atgme.org/). Following the 6xHis tag, the *Eco*RI restriction enzyme site was added to the 3' end of the coding sequence, and the *Not*I restriction enzyme site was added to the 5' end. The coding sequence was generated by recursive PCR (rPCR) using synthetic oligonucleotides (Sentebiolab, Türkiye). The rPCR product and pPICZαA were double-digested with *Not*I and *Eco*RI and ligated using T4 DNA ligase to generate recombinant plasmid pPICZαA-385P.

The recombinant pPICZαA-385P was cloned into *E. coli* DH5α cells (Invitrogen, USA) by heat-shock process. The cells were then grown at 37°C in LB medium (10 g/L tryptone, 10 g/L NaCl, and 5 g/L yeast extract) supplemented with 25 μg/mL Zeocin (Invitrogen, USA) for 18-24 hours. Positive clones were verified by PCR using GFP (GAGAGGCTGAAGCTGAATTC)/GRP (TTGGTTCTAGAAAGCTTGCGG) primers specific to inserted DNA fragment encoding the 385P peptide. In addition, an approximately 681-bp fragment amplified using the 5′ AOX1 (GACTGGTTCCAATTGACAAGC) and 3′ AOX1 (GCAAATGGCATTCTGACATCC) primers were sequenced to confirm the correct insertion and sequence integrity of the 385P coding sequence. The verified plasmid was linearized with *Sac*I (TransGen Biotech, China) and transformed into *P. pastoris* GS115 (Invitrogen, USA) by electroporation at 1.5 kV for 5 ms (MicroPulser™, Bio-Rad, USA). Transformants were selected on YPDS agar containing 200 μg/mL Zeocin after incubation at 30°C for 3–5 days. Integration of the expression cassette into the AOX1 locus was confirmed by PCR using both the GFP/GRP and 5′ AOX1/3′ AOX1 primers, and transcription was verified by RT-PCR. The confirmed strains were designated *P. pastoris* GS115/pPICZαA-385P.

2.4. Expression, purification, and quantification of recombinant 385P

Recombinant 385P (r385P) was expressed in *P. pastoris* GS115/pPICZαA-385P according to the EasySelect™ *Pichia* Expression Kit protocol (Invitrogen, China). Transformants were cultured in 50 mL buffered glycerol complex medium [BMGY; 1% yeast extract, 2% peptone, 100 mM potassium phosphate, pH 6.0, 1.34% YNB (yeast nitrogen base without amino acids)] at 30°C and 250 rpm for 16–18 h to an OD_{600} of 2–6, harvested by centrifugation (3,000 × g, 10 min), and resuspended in buffered methanol complex medium [BMMY; 1% yeast extract, 2% peptone, 100 mM potassium phosphate, pH 6.0, 1.34% YNB, 0.005% biotin, and 0.5% methanol] to an OD_{600} of 1. Expression was induced at 30°C and 250 rpm for 96 h by adding methanol every 24 h to a final concentration of 1% (v/v). Secreted r385P was separated by Tricine SDS-PAGE [33], transferred to a PVDF membrane, and visualized using a ChemiDoc Imaging System (Bio-Rad, USA).

After induction, the culture was centrifuged at 12,000 × g for 20 min at 4°C, and r385P in the cell-free supernatant was precipitated with 60% (w/v) ammonium sulfate and recovered by centrifugation at 25,000 × g for 15 min at 4°C [34]. The pellet was dissolved in 30 mM Tris buffer (pH 7.4) and sequentially purified using Sephadex G-25 and G-10 columns (5 × 100 mm) with 30 mM Tris buffer (pH 7.4) at a flow rate of 0.3 mL/min.

The purified r385P was quantified using a competitive His-Tag ELISA kit (GenScript, L00436, USA). A standard curve was generated using 6×His-tag standards (0–729 ng/mL), and absorbance was measured at 450 nm after development with 3,3′,5,5′-tetramethylbenzidine (TMB). The r385P concentration was determined by interpolation from the standard curve.

2.5. Circular Dichroism Spectroscopy and Secondary Structure Analysis

The secondary structure of r385P was analyzed by far-UV circular dichroism (CD) spectroscopy using a JASCO J-815 spectropolarimeter (Jasco Instruments, Canada). The peptide was dissolved at 100 μM in 10 mM sodium phosphate buffer (pH 7.5) and placed in a 1-cm quartz cuvette. CD spectra were recorded from 195 to 260 nm at a scan rate of 100 nm/min and a data pitch of 0.1 nm. The secondary structure composition was estimated using the BeStSel (Beta Structure Selection https://bestsel.elte.hu/index.php) deconvolution algorithm, and the quality of the spectral fit was assessed by the normalized root-mean-square deviation (NRMSD).

2.6. Analysis of antimicrobial activity

The minimum inhibitory concentration (MIC) values of r385P against pathogenic bacterial and yeast strains were determined by the broth microdilution method according to the Clinical and Laboratory Standards Institute guidelines [35]. Bacterial cultures in the logarithmic growth phase were adjusted to an OD_{600} of 0.2–0.3 and diluted 1:100 in Mueller-Hinton broth (MHB), whereas yeast cultures were adjusted to 0.5 McFarland and diluted 1:100 in malt extract broth (MEB). The cultures were inoculated into 96-well polystyrene plates containing two-fold serial dilutions of r385P (2–256 μg/mL) and incubated for 18–24 h at 37°C for bacteria and 35°C for yeasts. Untreated cultures served as positive controls, while sterile LB and MEB media served as negative controls. After incubation, absorbance was measured at 600 nm using a microplate reader (Thermo Fisher Scientific, USA), and the MIC was defined as the lowest r385P concentration that completely inhibited microbial growth.

2.7. Synergy Analysis Using Fractional Inhibitory Concentration Index (FICI)

Synergistic interactions between the 385P peptide and a group of antibiotics were evaluated using the standard checkerboard method [36]. In the assay, the antibiotic was serially diluted twofold along the x-axis, whereas r385P was serially diluted twofold along the y-axis, with the initial concentrations set to their respective MIC values. Each well received 50 μL of the bacterial suspension (*E. coli* ATCC 25922), and the final volume was adjusted to 100 μL with Mueller–Hinton broth. The fractional inhibitory concentration index (FICI) was calculated as follows: FICI = (MIC of the antibiotic in combination/MIC of the antibiotic alone) + (MIC of r385P in combination/MIC

of r385P alone). Drug interactions were interpreted as synergistic (FICI ≤ 0.5), additive (0.5 < FICI ≤ 1), indifferent (1 < FICI < 2), or antagonistic (FICI ≥ 2).

2.8. Antibiofilm activity analysis

The inhibitory effect of r385P on biofilm formation by *S. aureus* ATCC 29213 and *E. coli* O157:H7 ATCC 43894 was evaluated using a static microtiter plate assay as described by Kwasny and Opperman [37], with minor modifications. Overnight cultures were diluted in LB broth to approximately 5 × 10^6 CFU/mL and added to 96-well polystyrene plates containing two-fold serial dilutions of r385P (8–64 µg/mL). Untreated bacterial cultures and uninoculated medium served as the untreated biofilm growth and uninoculated background controls, respectively. Following static incubation at 37°C for 24 h, the wells were washed twice with sterile phosphate-buffered saline (PBS), heat-fixed at 60°C for 1 h, and stained with 0.1% (w/v) crystal violet for 15 min at room temperature. After washing with distilled water and air-drying, biofilm-bound crystal violet was solubilized with 33% (v/v) acetic acid, and absorbance was measured at 600 nm using a microplate reader (Thermo Fisher Scientific, USA). Experiments were performed in three independent biological replicates, each with three technical replicates. Biofilm inhibition was calculated relative to the untreated control as follows:

$$\text{Biofilm inhibition (\%)} = \left(1 - \frac{\text{Asample} - \text{Ablank}}{\text{Acontrol} - \text{Ablank}}\right) \text{X}100$$

where *A*sample, *A*control, and *A*blank represent the absorbance values of peptide-treated biofilms, untreated biofilm growth controls, and uninoculated medium controls, respectively. The minimum biofilm inhibitory concentration (MBIC) was defined as the lowest r385P concentration that reduced biofilm biomass by ≥80% relative to the untreated control.

2.9. Hemolytic activity and cytotoxicity

The hemolytic activity of r385P was evaluated using mouse erythrocytes as described by Meng et al. [38]. The study was approved by the Local Ethics Committee for Animal Experiments at Erciyes University (HADYEK; approval no. 22/110, 01/06/2022). Erythrocytes were collected by centrifugation at 1500 × g for 5 min and washed three times with 10 mM PBS (pH 7.4). The erythrocyte suspension was adjusted to 4% (v/v) in PBS and mixed with r385P (4–256 µg/mL) at a 1:10 (v/v) ratio. After incubating at 37 °C for 30 min, the suspensions were centrifuged at 4000 rpm for 5 min, the absorbance of the supernatant was measured at 450 nm. Triton X-100 (1%,

v/v) and 10 mM PBS served as positive (100% hemolysis) and negative (0% hemolysis) controls, respectively. Hemolysis was calculated as follows:

$$\text{Hemolysis (\%)}=\left(\frac{\text{Asample} - \text{A0}}{\text{A100} - \text{A0}}\right) \text{X100}$$

where *A*sample, *A*0, and *A*100 represent the absorbance values of the r385P-treated sample, negative control, and positive control, respectively.

The cytotoxicity of r385P was assessed against MRC-5 human lung fibroblast cells using the MTT assay [39]. Cells were cultured in Dulbecco's Modified Eagle's Medium (DMEM) supplemented with 10% fetal bovine serum (FBS) at 37°C in 5% CO_2 and seeded into 96-well plates at 1×10^4 cells/well. After 24 h of attachment, the cells were treated with r385P (5–320 µg/mL) for 48 h. The medium was then replaced with 100 µL of fresh medium and 100 µL of MTT solution (5 mg/mL in PBS). After a 4-h incubation, the MTT-containing medium was removed and the formazan crystals were dissolved in 100 µL DMSO. Absorbance was measured at 540 nm using a microplate spectrophotometer (Allsheng AMR-100, China). Untreated cells and culture medium alone served as positive and negative controls, respectively. All assays were performed in triplicate, and cell viability was calculated as follows:

$$\text{Cell viability (\%)}=\left(\frac{\text{A540 nm treated cells}}{\text{A540 nm untreated cells}}\right) \text{X100}$$

2.10. Stability profile of the r385P peptide

The stability profile of the r385P peptide was assessed through thermal stability, protease resistance, and salt tolerance experiments following established protocols [40]. Thermal stability was evaluated by incubating peptide solutions (0-128 µg/mL) at four different temperatures (4°C, 24°C, 65°C, and 95°C) for 1 h. Protease resistance was determined by incubating the r385P peptide with trypsin (13,000-20,000 U/mg, Sigma, T0303-1G, USA) in 100 mM Tris-HCl buffer (pH 7.0) at a 1:1 (v/v) ratio for 4 h at 37°C, followed by enzyme inactivation at 65°C for 10 min. Salt tolerance was assessed by incubating r385P with 50, 150, and 200 mM NaCl for 1 h. Following each treatment, antimicrobial activity was determined by measuring the MIC against *E. coli* ATCC 25922, with untreated r385P serving as the control.

3. RESULTS AND DISCUSSION

3.1. Physicochemical Characterization of 385P

The designed antimicrobial peptide, 385P comprised 36 amino acid residues and had a predicted molecular weight of 4321.9 Da. In terms of sequence length, 385P is longer than classical insect PrAMPs such as apidaecin, drosocin, oncocin, and pyrrhocoricin, which typically consist of 18–20 amino acids with molecular weights of approximately 2.1–2.4 kDa. Its length is more comparable to that of abaecin, a 34-residue PrAMP from *Apis mellifera*, and mammalian PrAMPs such as Bac7 and PR-39, which comprise approximately 35–39 residues. Despite its greater length, 385P retained a high proline content, with 11 proline residues accounting for 30.6% of its sequence, consistent with the 25–40% typically reported for naturally occurring PrAMPs. Addition of a C-terminal 6×His tag for recombinant production yielded a 42-residue peptide (r385P) with a predicted molecular weight of 5144.75 Da and reduced the relative proline content to 26.2%, which remained within the characteristic range of PrAMPs. High proline content is a defining feature of this peptide class and generally suppresses the formation of stable α-helical structures while favoring flexible polyproline type II (PPII)-like conformations that can facilitate interactions with intracellular targets such as the bacterial 70S ribosome and DnaK.

The net positive charge of both the 385P (+7.2) and r385P (+7.8) peptides also falls within the range commonly reported for naturally occurring PrAMPs. Cationicity is an essential physicochemical feature of antimicrobial peptides because it promotes the initial electrostatic interaction with the negatively charged bacterial cell envelope. However, unlike membrane-active antimicrobial peptides, excessive positive charge is not considered the principal determinant of PrAMP activity, as efficient intracellular transport and subsequent interaction with ribosomal or chaperone targets are primarily responsible for their antibacterial effects. The predicted pI values for both 385P and r385P were 11.73, indicating that the peptides remain highly cationic at physiological pH. This physicochemical property is expected to facilitate electrostatic interactions with the negatively charged bacterial cell surface, a prerequisite for the transporter-mediated intracellular uptake characteristic of proline-rich antimicrobial peptides.

The calculated hydrophobicity values of the core 385P and recombinant r385P peptides were 0.368 and 0.334, respectively, indicating that both peptides possess moderate hydrophobicity. Moderate hydrophobicity is a common feature of proline-rich antimicrobial peptides and distinguishes them from many membrane-active antimicrobial peptides, which generally require higher hydrophobicity to facilitate membrane insertion and disruption. In contrast, PrAMPs primarily rely on electrostatic interactions with the bacterial cell surface followed

by transporter-mediated uptake into the cytoplasm. Therefore, the moderate hydrophobicity observed for both 385P and r385P is consistent with the characteristic non-lytic mechanism of action of this peptide family.

3.2. Cloning and transformation

The 385P coding sequence was assembled from two synthetic 83-bp overlapping oligonucleotides by recursive PCR. Agarose gel electrophoresis confirmed amplification of the expected 151-bp product (Fig. 2A). The purified PCR product was successfully ligated into the pPICZαA expression vector to generate the recombinant plasmid pPICZαA-385P. Following transformation into *E. coli* DH5α, positive clones were confirmed by PCR using the GFP/GRP and 5′ AOX1/3′ AOX1 primer pairs, and the expected 151- and 681-bp bands were observed, respectively (Fig. 2B). DNA sequencing of the recombinant construct further demonstrated 100% sequence identity to the expected AOX1 region of the pPICZαA vector, which contains the 385P coding sequence.

Following linearization and transformation into *P. pastoris* GS115, positive transformants were identified by PCR using the GFP/GRP primers, with the expected 151-bp band observed (Fig. 2C). In addition, PCR using the 5′ AOX1/3′ AOX1 primer pair revealed two bands of approximately 681 and 2,200 bp, corresponding to the integrated expression cassette and endogenous AOX1 locus, respectively. This amplification pattern confirmed integration at the AOX1 locus and was consistent with the Mut^+ phenotype. RT-PCR further yielded the expected 151-bp product, confirming transcription of the 385P coding sequence in *P. pastoris* GS115 (Fig. 2D).

3.3. Expression and Characterization of Recombinant 385P

Following 96 h of methanol induction, the culture medium was analyzed by SDS–PAGE using a 4–16% gradient gel, and protein bands were visualized by silver staining (Fig. 3A). A distinct band at approximately 5 kDa was observed, consistent with the predicted molecular weight of r385P (5.14 kDa). The identity of r385P was further confirmed by Western blotting using an anti-His antibody, which specifically detected the peptide (Fig. 3B).

After purification, r385P was quantified using a competitive His-tag ELISA. The calibration curve generated using His-tag standards showed good linearity ($R^2 = 0.983$) and was described by the equation y =2.0647x-0,589 (Fig. 3C). Based on this calibration curve, the concentration of purified r385P was determined to be 960 ± 31.60 mg/L. These findings confirmed the successful expression and secretion of r385P by *P. pastoris* cells.

The secondary structural characteristics of peptide r385P were investigated using far-UV CD spectroscopy. The CD spectrum recorded between 195 and 260 nm exhibited a pronounced negative band positioned around 208–

210 nm, while the characteristic double minima at 208 and 222 nm, typically associated with well-defined α-helical structures, were not observed. Additionally, the spectrum did not display a distinct negative band near 218 nm, which is generally indicative of β-sheet conformations. These spectral features suggest that peptide r385P does not adopt a highly ordered secondary structure in aqueous solution but instead exists predominantly in a flexible, largely disordered conformation. To quantify the secondary structure composition of r385P, the experimental CD spectrum was analyzed using the BeStSel deconvolution algorithm. The analysis revealed that r385P consists mainly of disordered structures (63.6%), with moderate contributions from antiparallel β-structures (20.6%) and smaller fractions of α-helical elements (8.0%) and turn structures (7.8%). The spectral fitting quality was high, as indicated by an NRMSD value of 0.037, demonstrating strong agreement between the experimental and predicted spectra.

The predominance of disordered structures observed in the BeStSel analysis is consistent with the overall shape of the CD spectrum, which is characterized by a single dominant minimum near 208 nm and the absence of the typical helical double minima. These spectral characteristics are frequently observed in peptides that exist primarily in random-coil or intrinsically disordered conformations in aqueous environments.

Importantly, similar CD spectral profiles have been reported for PrAMPs, which frequently exhibit limited secondary structure in solution due to the structural constraints imposed by proline residues. Proline residues are known to disrupt α-helical and β-sheet formation by introducing conformational rigidity to the peptide backbone, thereby promoting flexible coil-like structures. Previous studies have shown that many PrAMPs remain largely unstructured or weakly structured in aqueous environments, while they may adopt more ordered conformations when interacting with bacterial ribosomes, chaperone proteins such as DnaK, or other intracellular targets [14, 8, 41].

Taken together, the experimental CD spectrum and the BeStSel secondary-structure analysis consistently demonstrate that peptide r385P predominantly adopts a coil-dominated, conformationally flexible structure in aqueous solution, with only minor contributions from α-helical and β-structural elements. This structural profile is similar to those reported for other PrAMPs, supporting the idea that peptide r385P has the structural features typical of flexible bioactive peptides that can interact with multiple biological targets.

3.5. Antimicrobial activity of r385P

The antimicrobial activity of r385P was evaluated against a panel of Gram-negative and Gram-positive pathogenic bacteria using the broth microdilution method. r385P exhibited broad antibacterial activity, with MIC values ranging from 4 to 32 μg/mL (0.80–6.44 μM) against Gram-negative bacteria and from 2 to 32 μg/mL (0.40–6.44 μM) against Gram-positive bacteria (Fig. 4A). Among the Gram-negative strains, *Acinetobacter baumannii* EUCC-D1071 was the most susceptible, followed by *Escherichia coli* ATCC 25922 and *Salmonella enterica* serovar Typhimurium ATCC 14028. The highest activity against Gram-positive bacteria was observed for *Listeria monocytogenes* ATCC 7644, which exhibited the lowest MIC among the strains tested. In addition to its antibacterial activity, r385P inhibited the pathogenic yeasts *Candida albicans* ATCC 10231 and *Candida glabrata* EUCC-15M190, with an MIC of 64 μg/mL (12.88 μM) for both strains (Fig. 4A).

In the design of the peptide 385P, five conserved motifs with lengths ranging from 4 to 9 amino acids were incorporated. These motifs were derived from three well-characterized proline-rich antimicrobial peptides: Pyrrhocoricin, Drosocin-1, and Myticalin A6. Specifically, the motifs GSYLPRP (residues 4–10) and PIYN (residues 15–18) originated from Pyrrhocoricin; PRPYSPR (residues 3–9) and TSHPRPIRV (residues 11–19) were taken from Drosocin-1; and YPRWPRHP (residues 3–10) was obtained from Myticalin A6. Antimicrobial activity assays demonstrated that r385P exhibited markedly lower MIC values than those previously reported for its parent peptides, showing enhanced potency against common pathogens including *S. aureus*, *E. coli*, *S.* Typhimurium, *K. pneumoniae*, and *P. aeruginosa* [43, 44, 45, 46].

Findings from the literature clearly demonstrate that the region essential for the antibacterial activity of pyrrhocoricin is located between Asp2 and Pro10 [47]. Flexible docking analyses revealed that pyrrhocoricin is positioned near the D-E helix region of DnaK, with the Tyr6–Pro10 hexapeptide segment (YLPRP) establishing the most intimate contacts with the protein [48]. In this context, the designed peptide 385P incorporates an extended Gly4–Pro10 motif (GSYLPRP), which encompasses the critical YLPRP motif, implicated in direct and specific interactions with both the ribosome and DnaK [6]. Furthermore, given that the YLPRP motif of pyrrhocoricin has been identified as a pharmacophoric motif homologous to the YSPRP motif in drosocin [49], the coexistence of both motifs within the designed 385P peptide may potentiate its functional impact.

The designed peptide incorporates two conserved motifs, PIYN from Pyrrhocoricin and SHPRPIRV from Drosocin, which are known to facilitate membrane penetration and intracellular delivery. These cell-penetrating

modules likely serve as initial contact points with bacterial membranes, thereby enhancing both membrane interactions and intracellular target recognition [47].

The inclusion of the myticalin-derived 'YPRWPRHP' motif in our peptide design was a strategic choice to leverage the potent membrane-targeting properties based on its high aromatic residue content. This motif is rich in both Tyr (Y) and Trp (W) residues, which are collectively established as critical for membrane permeabilization [50]. While the presence of both aromatic residues is essential for the initial amphipathic character and membrane interaction, previous findings have demonstrated a functional hierarchy between these residues, indicating that the indole group of tryptophan plays a more critical role in the observed antimicrobial activity against *E. coli* and *P. aeruginosa* than the phenol group of tyrosine [46].

Proline residues within antimicrobial peptides may introduce hinge-like structural elements that increase conformational flexibility and influence peptide–membrane interactions. For example, the central PXXP hinge motifs in the membrane-active peptides HPA3P2 and PMAP-23 (PKLP and PQKP, respectively) have been reported to enhance structural flexibility, thereby improving antimicrobial activity and selectivity through dynamic interactions with bacterial membranes [51, 52]. In this study, the centrally located PRWP motif of the designed peptide 385P may serve an analogous structural role, contributing to the peptide's bioactivity, stability, and functional versatility.

The antimicrobial spectrum of r385P can be further evaluated in relation to the parental PrAMPs from which its functional motifs were derived. For example, pyrrhocoricin and drosocin are insect-derived PrAMPs that predominantly exhibit activity against Gram-negative bacteria. In comparative susceptibility assays, drosocin and pyrrhocoricin displayed MIC values of 2 and 8 μM, respectively, against *E. coli* BL21AI, whereas both peptides showed markedly weaker activity against *S. aureus* DSM 6247, with MIC values exceeding 32 μM [53]. In contrast, Myticalin A6 exhibited a distinct activity profile, with greater activity against Gram-positive bacteria. An MIC of 8 μg/mL (1.9 μM) was reported against *S. aureus* NBRC12732, compared with substantially higher values of 64 μg/mL (15.1 μM) against *E. coli* NBRC12734 and >128 μg/mL (>30.2 μM) against *P. aeruginosa* NBRC3080 [46]. These comparisons suggest that the rational combination of sequence motifs derived from pyrrhocoricin, drosocin, and Myticalin A6 may have broadened the antibacterial spectrum beyond that typically associated with the individual parental PrAMPs. The pyrrhocoricin- and drosocin-derived regions may contribute

to the characteristic activity against Gram-negative bacteria, whereas incorporation of the myticalin A6-derived motif may contribute to activity against Gram-positive organisms. Importantly, r385P was active not only against *E. coli* and *S.* Typhimurium, which are generally susceptible to classical PrAMPs, but also against *A. baumannii*, *K. pneumoniae*, *P. aeruginosa*, *S. aureus*, MRSA, *B. cereus*, and *L. monocytogenes*. This broadened activity profile is consistent with the underlying design rationale of combining functional regions from PrAMPs with complementary antimicrobial spectra.

3.6. FICI analysis

The interactions of r385P with different antibiotics against *K. pneumoniae* EUCC-D876, *P. aeruginosa* EUCC-D1233, and MRSA ATCC 43300 were evaluated using the FICI method. The interaction profiles varied depending on both the antibiotic and bacterial strain tested (Fig. 4B). In combination with gentamicin, r385P exhibited an additive interaction against *K. pneumoniae* (FICI = 0.625), whereas an antagonistic interaction was observed against *P. aeruginosa* (FICI = 2.0). The antagonistic interaction may reflect the intrinsic resistance mechanisms of *P. aeruginosa*, including its low outer membrane permeability, active efflux systems, and consequently reduced intracellular accumulation of aminoglycosides [54, 55]. Against MRSA, the r385P–gentamicin combination showed an indifferent interaction (FICI = 1.125), indicating no substantial enhancement of antibacterial activity. Tetracycline showed the most consistent interaction profile, with an FICI of 0.75 against all tested strains, indicating additive interactions with r385P. In contrast, kanamycin exhibited species-dependent effects, ranging from synergistic against *K. pneumoniae* (FICI = 0.375) to additive against MRSA (FICI = 0.75) and antagonistic against *P. aeruginosa* (FICI = 2.0). Similar variability has been reported for other PrAMP–antibiotic combinations. For example, Otvos et al. [19] reported strong synergy between the modified PrAMP A3-APO and colistin against *K. pneumoniae* and *A. baumannii* (ΣFIC = 0.08), whereas its combination with imipenem was additive against *K. pneumoniae* (FICI = 0.53). These findings indicate that the effects of PrAMP–antibiotic combinations are highly dependent on both the antibiotic and bacterial species and support further investigation of r385P in combination with conventional antibiotics.

In combination with ciprofloxacin, r385P exhibited antagonistic, additive, and indifferent interactions against *K. pneumoniae* (FICI = 2.0), *P. aeruginosa* (FICI = 0.75), and MRSA (FICI = 1.125), respectively. Similarly, in combination with chloramphenicol, r385P exhibited an antagonistic interaction against *P. aeruginosa* (FICI = 2.0), whereas indifferent and additive interactions were observed against *K. pneumoniae* (FICI = 1.0625) and MRSA

(FICI = 0.75), respectively. Overall, these findings indicate that antibiotic–r385P interactions may be influenced by differences in bacterial susceptibility and the mechanisms of action of the combined agents. Synergy was observed for the kanamycin–r385P combination against *K. pneumoniae* (FICI = 0.375), whereas tetracycline consistently exhibited additive interactions across all tested bacterial strains. Although these results suggest the potential of r385P as an antibiotic adjuvant, antagonistic interactions, particularly against *P. aeruginosa*, highlight the need for careful selection and optimization of peptide–antibiotic combinations before therapeutic application.

3.7. Antibiofilm activity of r385P

The antibiofilm activity of r385P against *S. aureus* ATCC 29213 and *E. coli* O157 ATCC 43894 was evaluated using the crystal violet microtiter plate assay at concentrations ranging from 2×MIC to MIC/32 (Fig. 4C). r385P exhibited concentration-dependent inhibition of biofilm formation in both species. At 2×MIC and 1×MIC, calculated inhibition exceeded 100% for both bacteria, reflecting background-corrected absorbance values below the blank rather than inhibition beyond complete suppression. Notably, substantial inhibition was maintained at MIC/2, reaching 83.83 ± 2.19% for *E. coli* and 96.59 ± 1.18% for *S. aureus*. Inhibition declined to 19.01 ± 5.95% and 8.18 ± 1.91%, respectively, at MIC/32. Peptide concentration significantly affected biofilm inhibition in both species (one-way ANOVA, $p < 0.001$). Based on a ≥90% inhibition threshold, the MBIC was estimated at 1×MIC (3.22 μg/mL) for *E. coli* and MIC/2 (3.22 μg/mL) for *S. aureus*. These findings demonstrate the concentration-dependent antibiofilm activity of r385P, including substantial inhibition at sub-MIC concentrations.

Biofilm formation enhances bacterial persistence and tolerance to antimicrobial agents, complicating the treatment of biofilm-associated infections. In this study, r385P exhibited strong concentration-dependent antibiofilm activity against both *E. coli* O157 and *S. aureus*, with substantial inhibition maintained at sub-MIC concentrations, particularly against *S. aureus*. Although the MBIC was 3.22 μg/mL for both species, this concentration corresponded to the MIC for *E. coli* and MIC/2 for *S. aureus*. These findings suggest that susceptibility to biofilm inhibition may differ from planktonic antimicrobial susceptibility, potentially reflecting species-specific differences in biofilm formation.

Antimicrobial peptides can inhibit biofilm formation through multiple mechanisms, including interference with bacterial adhesion, quorum sensing, extracellular polymeric substance (EPS) production, and biofilm-associated gene expression [56]. For example, LL-37 suppresses *P. aeruginosa* biofilm formation by affecting quorum sensing and bacterial attachment [57,58], whereas human β-defensin 3 reduces the expression of biofilm-

associated genes in *S. aureus* [59]. Although the underlying mechanism was not investigated, the substantial inhibition observed for r385P at MIC/2 (83.83% against *E. coli* and 96.59% against *S. aureus*) suggests that its antibiofilm activity may involve processes beyond planktonic growth inhibition.

The antibiofilm activity of r385P was also notable compared with previously reported peptides. Its MBIC of 3.22 μg/mL against both bacterial species was lower than the values reported for C14R against *S. aureus* (15.02 μg/mL) [60], NRC-16 and melittin against *P. aeruginosa* (8–35 μg/mL) [61], and the optimized peptide PSTO2-SR2 against *E. coli* (16.41 μg/mL) [62]. Although differences in bacterial strains and experimental conditions limit direct comparisons, these findings support the potential of r385P for controlling biofilm-associated contamination. Further studies involving established biofilm eradication assays, EPS quantification, and biofilm-associated gene expression analyses are needed to elucidate its antibiofilm mechanisms and assess its efficacy against mature biofilms.

3.8. Stability of r385P

The stability of r385P was evaluated under different proteolytic, saline, and thermal conditions by determining its residual antimicrobial activity against *E. coli* ATCC 25922. Notably, r385P exhibited resistance to trypsin treatment. Incubation with trypsin for 1, 2, and 4 h did not alter its antimicrobial activity, with the MIC remaining at 8 μg/mL at all tested time points (Fig. 4D). Proteolytic degradation is one of the major obstacles limiting the practical application of peptide-based antimicrobials, and even short cationic antimicrobial peptides can undergo substantial degradation by trypsin [63]. Protease stability has also been highlighted as a desirable feature of recently developed PrAMP-derived peptides intended for use in environments with high proteolytic activity [64]. The unchanged MIC following 4 h of trypsin exposure indicates that r385P retained its antibacterial activity under the tested conditions. However, further studies involving different proteolytic enzymes are needed to comprehensively assess its protease resistance.

r385P also exhibited high salt tolerance. The MIC remained unchanged at 8 μg/mL following exposure to 50, 150, and 200 mM NaCl, demonstrating retention of antibacterial activity throughout the tested concentration range (Fig. 4D). Salt sensitivity represents an important limitation for many AMPs because increasing ionic strength can weaken electrostatic interactions involved in peptide association with bacterial surfaces and consequently reduce antimicrobial activity. Indeed, physiological salts, particularly Na^+ and divalent cations, have been reported to

compromise the activity of several antimicrobial peptides [65]. This effect has also been described for PrAMPs. The proline-rich peptides OaBac5α and ChBac5 retained activity against several bacteria, including *E. coli* and *P. aeruginosa*, in the presence of 100 mM NaCl, although their activity against some other microorganisms was substantially reduced [66]. The stability of r385P across the tested NaCl concentrations suggests its potential suitability for applications under varying ionic conditions.

The MIC remained unchanged at 8 µg/mL after incubation at 4 and 24 °C for 1 h, whereas exposure to 65 and 95 °C increased the MIC to 16 and 32 µg/mL, respectively (Fig. 4D). Although elevated temperatures reduced its antibacterial potency, r385P retained activity even after exposure to 95 °C. This partial thermal stability may be associated with the conformational flexibility characteristic of PrAMPs, which often adopt predominantly disordered structures in aqueous environments [10]. However, the contribution of structural flexibility to thermal stability remains to be established. For comparison, the designed antimicrobial peptide R-FV-I16 was reported to retain activity against *E. coli* after incubation at 100 °C for 1 h [67].

3.9. Hemolytic Activity and Cytotoxicity Assay

The hemolytic activity of r385P was evaluated using fresh mouse erythrocytes. At the highest tested concentration (256 µg/mL), r385P induced only 3.99% hemolysis, indicating low hemolytic activity (Fig. 4E). Hemolysis below 5% is generally considered indicative of good hemocompatibility for antimicrobial peptides, suggesting that r385P possesses a favorable safety profile while retaining potent antimicrobial activity. The cytotoxicity of r385P was further evaluated using the human lung fibroblast cell line MRC-5. Cell viability remained at 100% at concentrations up to 80 µg/mL and decreased to 87% and 71% at 160 and 320 µg/mL, respectively (Fig. 4F). Notably, the highest tested concentration was five-fold greater than the maximum MIC (64 µg/mL) observed against the tested pathogens. Together, these findings indicate low hemolytic activity and limited cytotoxicity over the tested concentration ranges, supporting the potential of r385P for further antimicrobial development.

PR-AMPs are generally characterized by minimal toxicity in eukaryotic cells. Previous studies have demonstrated that peptides derived from both mammalian and insect PR-AMPs can be administered in animal models at concentrations substantially higher than their effective antimicrobial doses without observable adverse effects [8]. Consistently, low cytotoxicity and negligible hemolytic activity have been reported for a wide range of PR-AMPs in various mammalian cell lines, including Hep, HEK, and HeLa cells [68, 69, 70]. These findings are largely attributed to the limited ability of PR-AMPs to penetrate most eukaryotic cells. Moreover, PR-AMPs selectively

528 and efficiently inhibit the bacterial chaperone DnaK and its orthologs while exhibiting minimal cross-reactivity
529 toward human chaperones or other intracellular mammalian proteins, even when conjugated to cell-penetrating
530 peptides such as penetratin [53]. In support of this selectivity, human embryonic kidney HEK293 cells have been
531 reported to exhibit minimal cytotoxicity at PrAMP concentrations up to 600 μg/mL, while low hemolytic activity
532 has been observed in mouse and pig erythrocytes at concentrations up to 100 μM [45,71]. Similarly, apidaecin-1b
533 has been reported to exhibit limited cytotoxicity at relatively high concentrations, including 600 μg/mL in HeLa
534 cells [53] and 2000 μg/mL in HEK293 and HepG2 cells [72]. Although differences in peptide structure, cell type,
535 and assay conditions limit direct comparisons, these findings support the generally favorable selectivity profile of
536 PrAMPs.
537
538 **4. CONCLUSION**
539 Recently, proline-rich antimicrobial peptides (PrAMPs) have emerged as highly attractive candidates for next-
540 generation antimicrobial agent development due to their enhanced target selectivity and preferential binding to
541 intracellular targets rather than randomly disrupting membrane integrity. In this context, motif-based design
542 strategies that rely on conserved sequence elements capable of establishing strong interactions with specific
543 intracellular targets provide a robust framework for the rational design of novel PrAMPs with optimized biological
544 performance.
545
546 In this study, we established an end-to-end framework for the rational development of proline-rich antimicrobial
547 peptide (r385P), integrating motif-based peptide design, recombinant production in *P. pastoris* host cells, and
548 comprehensive biological characterization. Although several conserved motifs associated with the biological
549 activity of PrAMPs have been identified, and the potential cellular functions of some of these motifs have been
550 reported, their integration into a rational peptide design strategy has remained largely unexplored. To our
551 knowledge, this is the first study to identify and rank conserved sequence motifs from highly active PrAMPs
552 deposited in public databases using a motif discovery algorithm such as MEME, and to rationally assemble these
553 motifs to design novel PrAMPs. This integrated approach may contribute to the development of next-generation
554 antimicrobial peptides by providing a practical platform spanning computational motif discovery to experimentally
555 validated PrAMP candidates.
556

Experimental evaluation demonstrated that r385P exhibited potent and broad-spectrum antibacterial activity against both Gram-negative and Gram-positive bacteria, with particularly strong activity against *Listeria monocytogenes* and *Acinetobacter baumannii*. Notably, its activity extended beyond the Gram-negative bacteria typically susceptible to classical PrAMPs to include clinically and food-relevant Gram-positive pathogens, such as *S. aureus*, MRSA, *B. cereus*, and *L. monocytogenes*. This broadened activity profile may reflect the design rationale of combining functional regions derived from PrAMPs with complementary antimicrobial spectra. In addition, r385P exhibited strong antibiofilm activity. FICI analysis further revealed a pronounced synergistic interaction with kanamycin against *K. pneumoniae* and consistent additive interactions with tetracycline across all tested microorganisms, highlighting the potential of r385P as an adjuvant to selected conventional antibiotics. Importantly, its minimal hemolytic activity and low cytotoxicity toward mammalian cells support a favorable preliminary safety profile.

Overall, these findings demonstrate that the rational combination of conserved functional motifs derived from well-characterized PrAMPs represents a promising strategy for developing novel peptides with potent, broad-spectrum antimicrobial activity. Recombinant production of r385P in *P. pastoris* further demonstrates the feasibility of a microbial production platform that may offer an alternative to chemical synthesis, particularly for relatively long, proline-rich peptide sequences. Nevertheless, further studies are required to elucidate the molecular mechanism of action of r385P, define its structure–activity relationships and cellular uptake pathways, evaluate its stability and efficacy under physiologically relevant conditions, and establish its in vivo efficacy and safety.

Ethical Approval The protocol for the hemolytic activity assay using animal blood was approved by the Erciyes University Animal Experiments Local Ethics Committee (HADYEK) (Decision No: 22/110, Date: 01/06/2022).

Competing Interests The authors declare the following financial/commercial conflict of interest: The peptide sequences described in this study are protected by a granted patent by the Turkish Patent and Trademark Office (TÜRKPATENT) under registration number **2024/014075** (Title: *"Proline-Rich Antimicrobial Peptide"*). Aside from this, the authors declare no other known competing financial interests or personal relationships that could have appeared to influence the work reported in this paper.

References

587 1. Büyükkiraz ME, Kesmen Z (2022) Antimicrobial peptides (AMPs): a promising class of antimicrobial
588 compounds. J Appl Microbiol 132(3):1573–1596. https://doi.org/10.1111/jam.15314

589 2. Cao H, Ke T, Liu R, Yu J, Dong C, Cheng M et al (2015) Identification of a novel proline-rich antimicrobial
590 peptide from *Brassica napus*. PLoS One 10 (9): e0137414. https://doi.org/10.1371/journal.pone.0137414

591 3. Welch NG, Li W, Hossain MA, Separovic F, O'Brien-Simpson NM, Wade JD (2020) (Re)defining the
592 proline-rich antimicrobial peptide family and the identification of putative new members. Front Chem 8:607769.
593 https://doi.org/10.3389/fchem.2020.607769

594 4. Umumararungu T, Gahamanyi N, Mukiza J, Habarurema J, Katandula J, Rugamba A, Kagisha V (2024)
595 Proline, a unique amino acid whose polymer, polyproline II helix, and its analogues are involved in many
596 biological processes: a review. Amino Acids 56(1):50. https://doi.org/10.1007/s00726-024-03410-9

597 5. Adzhubei AA, Sternberg MJ, Makarov AA (2013) Polyproline-II helix in proteins: structure and function.
598 J Mol Biol 425 (12):2100–2132. https://doi.org/10.1016/j.jmb.2013.03.018

599 6. Brakel A, Krizsan A, Itzenga R, Kraus CN, Otvos L Jr, Hoffmann R (2022) Influence of substitutions in
600 the binding motif of proline-rich antimicrobial peptide ARV-1502 on 70S ribosome binding and antimicrobial
601 activity. Int J Mol Sci 23:3150. https://doi.org/10.3390/ijms23063150

602 7. Knappe D, Goldbach T, Hatfield M, Palermo N, Weinert S, Sträter N, Lovas S (2016) Proline-rich
603 antimicrobial peptides optimized for binding to *Escherichia coli* chaperone DnaK. Protein Pept Lett 23(6):1061–
604 1071. https://doi.org/10.2174/0929866523666160719124712

605 8. Scocchi M, Tossi A, Gennaro R (2011) Proline-rich antimicrobial peptides: converging to a non-lytic
606 mechanism of action. Cell Mol Life Sci 68 (13):2317–2330. https://doi.org/10.1007/s00018-011-0721-7

607 9. Mardirossian M, Grzela R, Giglione C, Meinnel T, Gennaro R, Mergaert P, Scocchi M (2014) The host
608 antimicrobial peptide Bac71-35 binds to bacterial ribosomal proteins and inhibits protein synthesis. Chem Biol
609 21(12):1639–1647. https://doi.org/10.1016/j.chembiol.2014.10.009

610 10. Mishra AK, Choi J, Moon E, Baek KH (2018) Tryptophan-rich and proline-rich antimicrobial peptides.
611 Molecules 23(4):815. https://doi.org/10.3390/molecules23040815

612 11. Krizsan A, Volke D, Weinert S, Sträter N, Knappe D, Hoffmann R (2014) Insect-derived proline-rich
613 antimicrobial peptides kill bacteria by inhibiting bacterial protein translation at the 70S ribosome. Angew Chem
614 Int Ed 53(45):12236–12239. https://doi.org/10.1002/anie.201407145

615 12. Krizsan A, Prahl C, Goldbach T, Knappe D, Hoffmann R (2015) Short proline-rich antimicrobial peptides
616 inhibit either the bacterial 70S ribosome or the assembly of its large 50S subunit. ChemBioChem 16(16):2304–
617 2308. https://doi.org/10.1002/cbic.201500375

618 13. Graf M, Wilson DN (2019) Intracellular antimicrobial peptides targeting the protein synthesis machinery.
619 In: Antimicrobial peptides: basics for clinical application. Springer, 73–89. https://doi.org/10.1007/978-981-13-
620 3588-4_6

621 14. Kragol G, Lovas S, Varadi G, Condie BA, Hoffmann R, Otvos L (2001) The antibacterial peptide
622 pyrrhocoricin inhibits the ATPase actions of DnaK and prevents chaperone-assisted protein folding. Biochemistry
623 40(10):3016–3026. https://doi.org/10.1021/bi002656a

624 15. Knappe D, Zahn M, Sauer U, Schiffer G, Sträter N, Hoffmann R (2011) Rational design of oncocin
625 derivatives with superior protease stabilities and antibacterial activities based on the high-resolution structure of
626 the oncocin-DnaK complex. ChemBioChem 12(6):874–876. https://doi.org/10.1002/cbic.201000792

627 16. Zahn M, Berthold N, Kieslich B, Knappe D, Hoffmann R, Sträter N (2013) Structural studies on the forward
628 and reverse binding modes of peptides to the chaperone DnaK. J Mol Biol 425(14):2463–2479.
629 https://doi.org/10.1016/j.jmb.2013.03.041

630 17. Scocchi M, Mardirossian M, Runti G, Benincasa M (2016) Non-membrane permeabilizing modes of action
631 of antimicrobial peptides on bacteria. Curr Top Med Chem 16(1):76–88.
632 https://doi.org/10.2174/1568026615666150703121009

633 18. Stączek S, Kunat-Budzyńska M, Cytryńska M, Zdybicka-Barabas A (2024) Proline-rich antimicrobial
634 peptides from invertebrates. Molecules 29(24):5864. https://doi.org/10.3390/molecules29245864

635 19. Otvos L Jr, Ostorhazi E, Szabo D, Zumbrun SD, Miller LL, Halasohoris SA, Kraus CN (2018) Synergy
636 between proline-rich antimicrobial peptides and small molecule antibiotics against selected gram-negative
637 pathogens in vitro and in vivo. Front Chem 6:309. https://doi.org/10.3389/fchem.2018.00309

20. Cui Q, Yu HD, Xu QJ, Liu Y, Wang YT, Li PH, Ma HX (2023) Antibiotic synergist OM19r reverses aminoglycoside resistance in multidrug-resistant *Escherichia coli*. Front Microbiol 14:1144946. https://doi.org/10.3389/fmicb.2023.1144946

21. Xuan J, Feng W, Wang J, Wang R, Zhang B, Bo L, Sun L (2023) Antimicrobial peptides for combating drug-resistant bacterial infections. Drug Resist Updat 68:100954. https://doi.org/10.1016/j.drup.2023.100954

22. Cassone M, Vogiatzi P, La Montagna R et al (2008) Scope and limitations of the designer proline-rich antibacterial peptide dimer, A3-APO, alone or in synergy with conventional antibiotics. Peptides 29(11):1878–1886. https://doi.org/10.1016/j.peptides.2008.07.016

23. Koch P, Schmitt S, Heynisch A, Gumpinger A, Wüthrich I, Gysin M, Held M (2022) Optimization of the antimicrobial peptide Bac7 by deep mutational scanning. BMC Biol 20(1):114. https://doi.org/10.1186/s12915-022-01304-4

24. Sadler K, Eom KD, Yang JL, Dimitrova Y, Tam JP (2002) Translocating proline-rich peptides from the antimicrobial peptide bactenecin 7. Biochemistry 41(48):14150–14157. https://doi.org/10.1021/bi0266611

25. Benincasa M, Scocchi M, Podda E, Skerlavaj B, Dolzani L, Gennaro R (2004) Antimicrobial activity of Bac7 fragments against drug-resistant clinical isolates. Peptides 25(12):2055–2061. https://doi.org/10.1016/j.peptides.2004.08.004

26. Mardirossian M, Sola R, Beckert B, Collis DW, Di Stasi A, Armas F, Scocchi M (2019) Proline-rich peptides with improved antimicrobial activity against *E. coli*, *K. pneumoniae*, and *A. baumannii*. ChemMedChem 14(24):2025–2033. https://doi.org/10.1002/cmdc.201900465

27. Bulet P, Hetru C, Dimarcq JL, Hoffmann D (1999) Antimicrobial peptides in insects; structure and function. Dev Comp Immunol 23(4-5):329–344. https://doi.org/10.1016/S0145-305X(99)00015-4

28. Podda E, Benincasa M, Pacor S, Micali F, Mattiuzzo M, Gennaro R, Scocchi M (2006) Dual mode of action of Bac7, a proline-rich antibacterial peptide. Biochim Biophys Acta Gen Subj 1760(11):1732–1740. https://doi.org/10.1016/j.bbagen.2006.09.006

29. Wibowo D, Zhao CX (2019) Recent achievements and perspectives for large-scale recombinant production of antimicrobial peptides. Appl Microbiol Biotechnol 103(2):659–671. https://doi.org/10.1007/s00253-018-9524-1

30. Li P, Anumanthan A, Gao XG, Ilangovan K, Suzara VV, Düzgüneş N, Renugopalakrishnan V (2007) Expression of recombinant proteins in *Pichia pastoris*. Appl Biochem Biotechnol 142(2):105–124. https://doi.org/10.1007/s12010-007-0003-x

31. Chen X, Li J, Sun H, Li S, Chen T, Liu G, Dyson P (2017) High-level heterologous production and functional secretion by recombinant *Pichia pastoris* of the shortest proline-rich antibacterial honeybee peptide Apidaecin. Sci Rep 7(1):14543. https://doi.org/10.1038/s41598-017-15149-3

32. Invitrogen (2016) EasySelect™ Pichia expression kit user guide. Doc. Part No. 25-0172, Cat. No. K174001. Thermo Fisher Scientific, Waltham, MA, USA

33. Schägger H (2006) Tricine–SDS-PAGE. Nat Protoc 1(1):16–22. https://doi.org/10.1038/nprot.2006.4

34. Büyükkiraz ME, Kesmen Z (2022) Recombinant expression and coexpression of oyster defensin and proline-rich peptide in *Komagataella phaffii*. Biotechnol Appl Biochem 69(5):1998–2007. https://doi.org/10.1002/bab.2262

35. CLSI (2018) Performance standards for antimicrobial susceptibility testing, 28th edn. CLSI supplement M100. Clinical and Laboratory Standards Institute, Wayne, PA

36. Li Q, Cebrián R, Montalbán-López M, Ren H, Wu W, Kuipers OP (2021) Outer-membrane-acting peptides and lipid II-targeting antibiotics cooperatively kill Gram-negative pathogens. Commun Biol 4(1):31. https://doi.org/10.1038/s42003-020-01511-1

37. Kwasny SM, Opperman TJ (2010) Static biofilm cultures of Gram-positive pathogens grown in a microtiter format used for anti-biofilm drug discovery. Curr Protoc Pharmacol 50(1):13A.8. https://doi.org/10.1002/0471141755.ph13a08s50

38. Meng DM, Li WJ, Shi LY, Lv YJ, Sun XQ, Hu JC, Fan ZC (2019) Expression, purification and characterization of a recombinant antimicrobial peptide Hispidalin in *Pichia pastoris*. Protein Expr Purif 160:19–27. https://doi.org/10.1016/j.pep.2019.03.007

39. Kesmen Z, Batman SG, Canpolat M, Büyükkiraz ME (2026) A localization-based motif combination approach to the design of antimicrobial peptides targeting Gram-positive and Gram-negative bacteria. Probiotics Antimicrob Proteins 1–18. https://doi.org/10.1007/s12602-025-10875-x

691 40. Batman SG, Kesmen Z (2025) Recombinant expression and functional characterization of defensin-like
692 peptide TEWP and its analogs in *Pichia pastoris*. World J Microbiol Biotechnol 41(10):392.
693 https://doi.org/10.1007/s11274-025-04745-5

694 41. Roy RN, Lomakin IB, Gagnon MG, Steitz TA (2015) The mechanism of inhibition of protein synthesis by
695 the proline-rich peptide oncocin. Nat Struct Mol Biol 22(6):466–469. https://doi.org/10.1038/nsmb.3031

696 42. Graf M, Mardirossian M, Nguyen F, Seefeldt AC, Guichard G, Scocchi M, Wilson DN (2017) Proline-rich
697 antimicrobial peptides targeting protein synthesis. Nat Prod Rep 34(7):702–711.
698 https://doi.org/10.1039/c7np00020k

699 43. Cociancich S, Dupont A, Hegy G, Lanot R, Holder F, Hetru C, Bulet P (1994) Novel inducible antibacterial
700 peptides from a hemipteran insect, the sap-sucking bug *Pyrrhocoris apterus*. Biochem J 300(2):567–575.
701 https://doi.org/10.1042/bj3000567

702 44. Menousek J, Mishra B, Hanke ML, Heim CE, Kielian T, Wang G (2012) Database screening and in vivo
703 efficacy of antimicrobial peptides against methicillin-resistant *Staphylococcus aureus* USA300. Int J Antimicrob
704 Agents 39(5):402–406. https://doi.org/10.1016/j.ijantimicag.2012.02.003

705 45. Knappe D, Cassone M, Nollmann FI, Otvos L, Hoffmann R (2014) Hydroxyproline substitutions stabilize
706 non-glycosylated drosocin against serum proteases without challenging its antibacterial activity. Protein Pept Lett
707 21(4):321–329. https://doi.org/10.2174/09298665113206660105

708 46. Okimura K, Matsubara K, Suzuki R, Ito H, Sato A, Sugimoto K (2021) Examination of the antimicrobial
709 peptide Myticalin A6 active site. Biol Pharm Bull 44(4):515–521. https://doi.org/10.1248/bpb.b20-00799

710 47. Kragol G, Hoffmann R, Chattergoon MA, Lovas S, Cudic M, Bulet P, Otvos L Jr (2002) Identification of
711 crucial residues for the antibacterial activity of the proline-rich peptide, pyrrhocoricin. Eur J Biochem
712 269(17):4226–4237. https://doi.org/10.1046/j.1432-1033.2002.03119.x

713 48. Otvos L (2002) The short, proline-rich antibacterial peptide family. Cell Mol Life Sci 59(7):1138–1150.
714 https://doi.org/10.1007/s00018-002-8493-8

715 49. Bencivengo AM, Cudic M, Hoffmann R, Otvos L Jr (2001) The efficacy of the antibacterial peptide,
716 pyrrhocoricin, is finely regulated by its amino acid residues and active domains. Lett Pept Sci 8(3):201–209.
717 https://doi.org/10.1023/A:1016200307296

718 50. Pacor S, Benincasa M, Musso MV, Krce L, Aviani I, Pallavicini A, Mardirossian M (2021) The proline-
719 rich myticalins from *Mytilus galloprovincialis* display a membrane-permeabilizing antimicrobial mode of action.
720 Peptides 143:170594. https://doi.org/10.1016/j.peptides.2021.170594

721 51. Lee JK, Park SC, Hahm KS, Park Y (2014) A helix-PXXP-helix peptide with antibacterial activity without
722 cytotoxicity against MDRPA-infected mice. Biomaterials 35(3):1025–1039.
723 https://doi.org/10.1016/j.biomaterials.2013.10.035

724 52. Lyu Y, Tan M, Xue M, Hou W, Yang C, Shan A, Cheng B (2023) Broad-spectrum hybrid antimicrobial
725 peptides derived from PMAP-23 with potential LPS binding ability. Biochem Pharmacol 210:115500.
726 https://doi.org/10.1016/j.bcp.2023.115500

727 53. Hansen A, Schäfer I, Knappe D, Seibel P, Hoffmann R (2012) Intracellular toxicity of proline-rich
728 antimicrobial peptides shuttled into mammalian cells by the cell-penetrating peptide penetratin. Antimicrob Agents
729 Chemother 56(10):5194–5201. https://doi.org/10.1128/AAC.00585-12

730 54. Poole K (2005) Aminoglycoside resistance in *Pseudomonas aeruginosa*. Antimicrob Agents Chemother
731 49(2):479–487. https://doi.org/10.1128/AAC.49.2.479-487.2005

732 55. Langendonk RF, Neill DR, Fothergill JL (2021) The building blocks of antimicrobial resistance in
733 *Pseudomonas aeruginosa*: implications for current resistance-breaking therapies. Front Cell Infect Microbiol
734 11:665759. https://doi.org/10.3389/fcimb.2021.665759

735 56. Di Somma A, Moretta A, Canè C, Cirillo A, Duilio A (2020) Antimicrobial and antibiofilm peptides.
736 Biomolecules 10(4):652. https://doi.org/10.3390/biom10040652

737 57. Overhage J, Campisano A, Bains M, Torfs ECW, Rehm BHA, Hancock REW (2008) Human host defense
738 peptide LL-37 prevents bacterial biofilm formation. Infect Immun 76(9):4176–4182.
739 https://doi.org/10.1128/IAI.00318-08

740 58. Mansour SC, Pena OM, Hancock REW (2014) Host defense peptides: front-line immunomodulators.
741 Trends Immunol 35(9):443–450. https://doi.org/10.1016/j.it.2014.07.004

742 59. Zhu C, Tan H, Cheng T, Shen H, Shao J, Guo Y, Shi S, Zhang X (2013) Human β-defensin 3 inhibits
743 antibiotic-resistant *Staphylococcus* biofilm formation. J Surg Res 183(1):204–213.
744 https://doi.org/10.1016/j.jss.2012.11.048

60. Gruber D, Vogel V, Walter JC, Bolotnikov G, Rodríguez A, Preising N, Ständker L, Firacative C, Spellerberg B, Kissmann AK, Rosenau F (2026) The antimicrobial peptide C14R is active against all pathogenic species of the ESKAPE group. Antibiotics 15(2):211. https://doi.org/10.3390/antibiotics15020211

61. Gopal R, Lee JH, Kim YG, Kim MS, Seo CH, Park Y (2013) Anti-microbial, anti-biofilm activities and cell selectivity of the NRC-16 peptide derived from witch flounder, *Glyptocephalus cynoglossus*. Mar Drugs 11(6):1836–1852. https://doi.org/10.3390/md11061836

62. Yin W, Yao J, Leng X, Ma C, Chen X, Jiang Y, Wang T, Chen T, Shaw C, Zhou M, Wang L (2024) Enhancement of antimicrobial function by L/D-lysine substitution on a novel broad-spectrum antimicrobial peptide, Phylloseptin-TO2: a structure-related activity research study. Pharmaceutics 16(8):1098. https://doi.org/10.3390/pharmaceutics16081098

63. Svenson J, Stensen W, Brandsdal BO, Haug BE, Monrad J, Svendsen JS (2008) Antimicrobial peptides with stability toward tryptic degradation. Biochemistry 47(12):3777–3788. https://doi.org/10.1021/bi7019904

64. Cappella G, Di Stasi A, Cortese C, Torrini L, D'Amore A, Niccolini V, de Pascale L, Casciaro B, Mardirossian M, Pini A, Mangoni ML, Scocchi M (2026) Two shorter variants of the proline-rich antimicrobial peptide B7-005 scaffold active against clinical isolates of *Pseudomonas aeruginosa* and *Staphylococcus aureus*. Antibiotics 15(4):412. https://doi.org/10.3390/antibiotics15040412

65. Xu S, Tan P, Tang Q, Wang T, Ding Y, Fu H, Zhang Y, Zhou C, Song M, Tang Q, Sun Z, Ma X (2023) Enhancing the stability of antimicrobial peptides: from design strategies to applications. Chem Eng J 475:145923. https://doi.org/10.1016/j.cej.2023.145923

66. Shamova O, Brogden KA, Zhao C, Nguyen T, Kokryakov VN, Lehrer RI (1999) Purification and properties of proline-rich antimicrobial peptides from sheep and goat leukocytes. Infect Immun 67(8):4106–4111. https://doi.org/10.1128/IAI.67.8.4106-4111.1999

67. Xu W, Zhu X, Tan T, Li W, Shan A (2014) Design of embedded-hybrid antimicrobial peptides with enhanced cell selectivity and anti-biofilm activity. PLoS One 9(6). https://doi.org/10.1371/journal.pone.0098935

68. Kolano L, Knappe D, Berg A, Berg T, Hoffmann R (2022) Effect of amino acid substitutions on 70S ribosomal binding, cellular uptake, and antimicrobial activity of Oncocin Onc112. ChemBioChem 23(5). https://doi.org/10.1002/cbic.202100609

69. Czihal P, Knappe D, Fritsche S, Zahn M, Berthold N, Piantavigna S, Hoffmann R (2012) Api88 is a novel antibacterial designer peptide to treat systemic infections with multidrug-resistant Gram-negative pathogens. ACS Chem Biol 7(7):1281–1291. https://doi.org/10.1021/cb300063v

70. Brakel A, Grochow T, Fritsche S, Knappe D, Krizsan A, Fietz SA, Müller U (2024) Evaluation of proline-rich antimicrobial peptides as potential lead structures for novel antimycotics against *Cryptococcus neoformans*. Front Microbiol 14:1328890. https://doi.org/10.3389/fmicb.2023.1328890

71. Tonk M, Pierrot C, Cabezas-Cruz A, Rahnamaeian M, Khalife J, Vilcinskas A (2019) The *Drosophila melanogaster* antimicrobial peptides Mtk-1 and Mtk-2 are active against the malarial parasite *Plasmodium falciparum*. Parasitol Res 118(6):1993–1998. https://doi.org/10.1007/s00436-019-06305-x

72. Berthold N, Czihal P, Fritsche S, Sauer U, Schiffer G, Knappe D et al (2013) Novel apidaecin 1b analogs with superior serum stabilities for treatment of infections by gram-negative pathogens. Antimicrob Agents Chemother 57(1):402–409. https://doi.org/10.1128/AAC.01923-12

Figure Captions

Figure 1. Design of the 385P peptide, showing the incorporated motifs and their corresponding parental peptides. Residues 2–8 were derived from Drosocin-1 (ID: DBAASPR_564), residues 9–15 and 33–36 from Pyrrhocoricin (ID: DBAASPR_1205), and residues 16–23 from Myticalin A6 (16–29) (ID: DBAASPS_18054).

Figure 2. Molecular construction and verification of recombinant r385P expression in *Pichia pastoris* GS115. (A) Confirmation of the 151-bp recursive PCR product encoding 385P by agarose gel electrophoresis. (B) Confirmation of recombinant pPICZαA-385P plasmid construction by PCR using 385P-specific GFP/GFR primers (a) and 5′AOX1/3′AOX1 primers (b). (C) Sequence analysis of the AOX region containing the 385P-coding sequence. (D) Confirmation of the integration of the 385P-coding sequence into the *P. pastoris* genome by PCR using 385P-specific GFP/GFR primers (a) and 5′AOX1/3′AOX1 primers (b). (E) Confirmation of transcription of the 385P-coding gene by RT-PCR using 385P-specific GFP/GFR primers (a) and 5′AOX1/3′AOX1 primers (b).

Figure 3. Characterization of r385P. A) SDS-PAGE analysis r385P. (B) Western blot analysis (C) Structural analysis: CD spectrum spectrum of r385P recorded between 195–260 nm İN 10mM sodium phosphate, pH 7.5

Secondary structure composition estimated using the BeStSel algorithm. D) His-Tag ELISA standard curve for r385 quantification

Figure 4. Biological activity, stability, and safety profile of r385P. (A) Antimicrobial activity of r385P against Gram-negative and Gram-positive bacteria and yeasts. MIC values are expressed in μg/mL, with the corresponding μM values given in parentheses. (B) Heatmap representation of FICI values for r385P in combination with conventional antibiotics. Each cell shows the concentrations of r385P and the corresponding antibiotic used in combination (μg/mL), with the resulting FICI value indicated in parentheses. (C) Antibiofilm activity of r385P against *S. aureus* ATCC 29213 and *E. coli* O157:H7 ATCC 43894 at different concentrations relative to the MIC. Biofilm inhibition is expressed as percentage inhibition relative to the control, and data are presented as mean ± SD. (D) Stability of r385P under thermal, salt, and proteolytic stress conditions. Residual antimicrobial activity was determined against *E. coli* ATCC 25922 following exposure to different temperatures (4, 24, 65, and 95 °C), NaCl concentrations (50, 150, and 200 mM), and trypsin treatment for 1, 2, and 4 h. (E) Hemolytic activity of r385P toward mouse erythrocytes. (F) Cytotoxicity of r385P toward MRC-5 human lung fibroblast cells determined by the MTT assay.

Abbreviations

AMP	Antimicrobial peptide
ATCC	American Type Culture Collection
CD	Circular dichroism
CLSI	Clinical and Laboratory Standards Institute
DBAASP	Database of Antimicrobial Activity and Structure of Peptides
DMEM	Dulbecco's Modified Eagle's Medium
DMSO	Dimethyl sulfoxide
DNA	Deoxyribonucleic acid
EPS	Extracellular polymeric substance
EUCC	Erciyes University Culture Collection
FBS	Fetal bovine serum
FICI	Fractional Inhibitory Concentration Index
h	Hour
LB	Luria-Bertani
MBIC	Minimum biofilm inhibitory concentration
MEB	Malt extract broth
MDR	Multidrug-resistant
MEME	Multiple Expectation Maximizations for Motif Elicitation
MHB	Mueller-Hinton broth
MIC	Minimum inhibitory concentration
min	Minute
mM	Millimolar
MRBC	Mouse red blood cells
MRSA	Methicillin-resistant *Staphylococcus aureus*
MTT	Methyl thiazol tetrazolium
NaCl	Sodium chloride
nm	Nanometer
NRMSD	Normalized root-mean-square deviation
OD	Optical density
PBS	Phosphate-buffered saline
PCR	Polymerase chain reaction
pI	Isoelectric point
PrAMP	Proline-rich antimicrobial peptides
rpm	Revolutions per minute
rPCR	Recursive polymerase chain reaction
RT-PCR	Reverse transcription polymerase chain reaction
SPPS	Solid-phase peptide synthesis
v	Volume
w	Weight

RATIONAL DESIGN STRATEGY OF 385P

1 Data Collection and Filtering



Proline-rich antimicrobial peptides **(PrAMPs)** were retrieved from DBAASP and filtered according to predefined selection criteria.

2 Motif Discovery (MEME Suite)



Conserved sequence motifs among **highly active PrAMPs** were identified and ranked using MEME Suite.

3 Biophysical and Computational Screening

HeliQuest



Evaluation of physicochemical properties

CAMP-R3



Prediction of antimicrobial potential

HemoPI2



Prediction of hemolytic activity

Candidate sequences were screened using **HeliQuest** for physicochemical properties, **CAMP-R3** for antimicrobial potential, and **HemoPI2** for hemolytic activity.

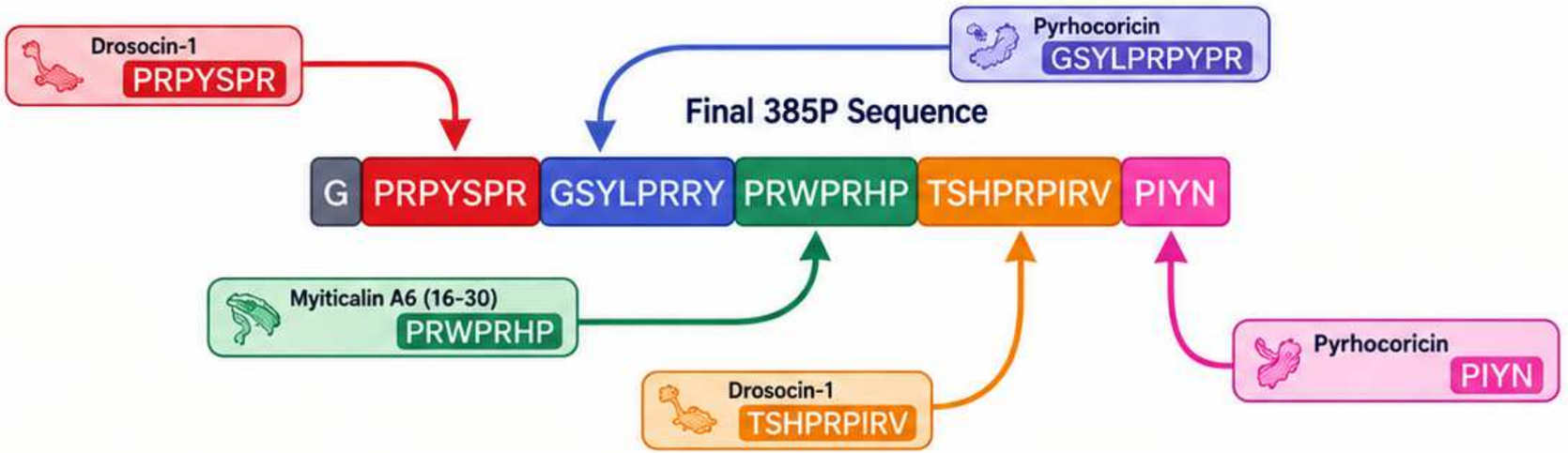
RATIONAL ASSEMBLY OF FUNCTIONAL MOTIFS IN 385P

Rational Motif Assembly

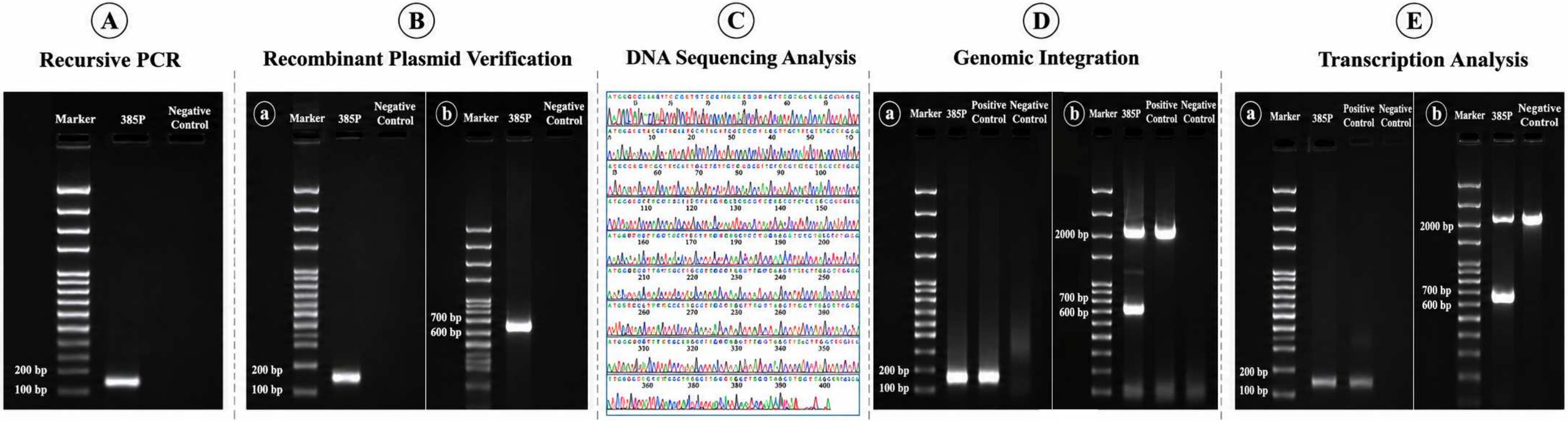
385P was rationally designed by combining selected functional motifs derived from three parental PrAMPs: **drosocin**, **pyrrhocoricin**, and **Myticalin A6**.

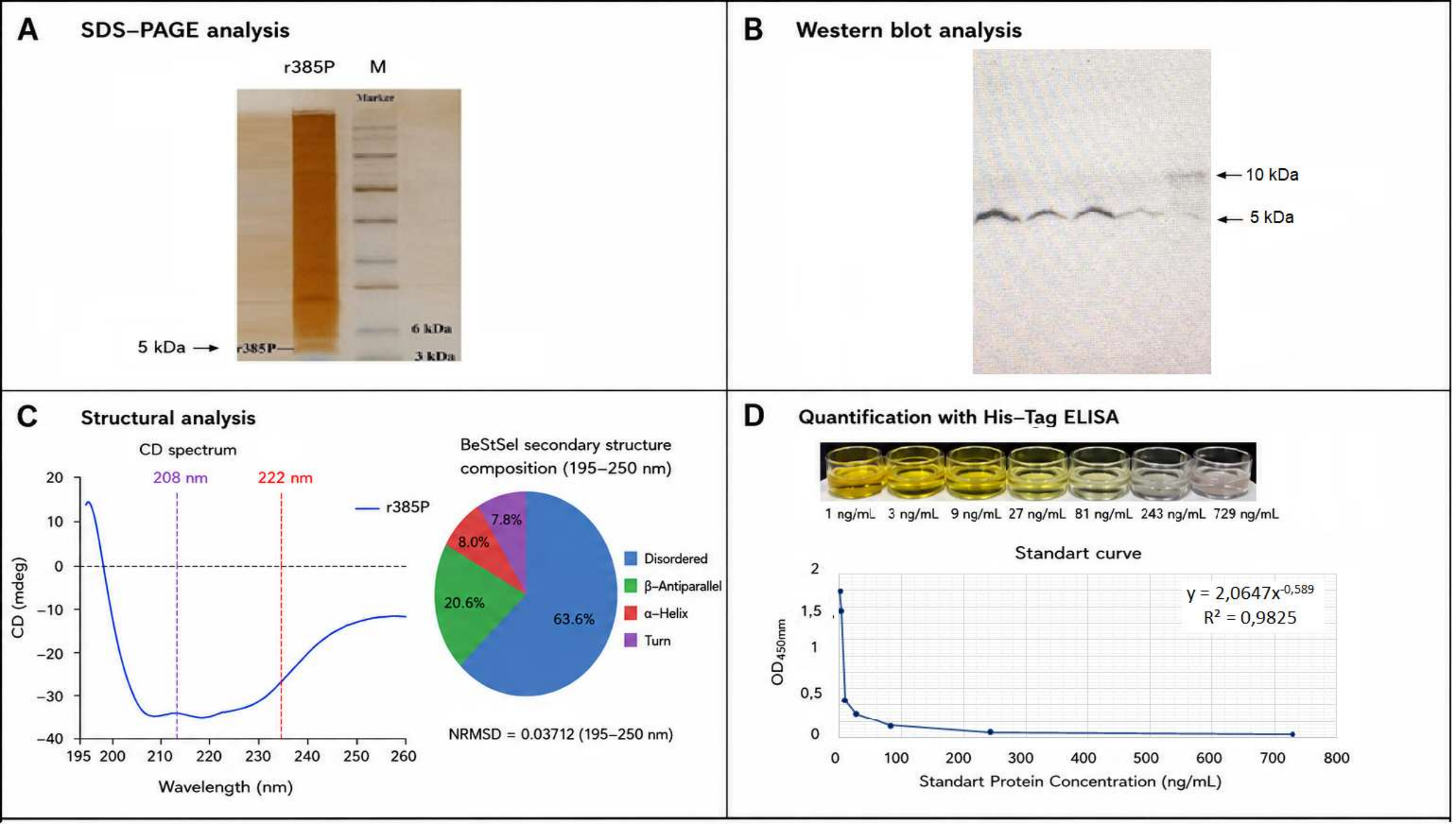
N N-Terminal Modification

A glycine (G) residue was introduced at the N-terminus of the designed sequence.

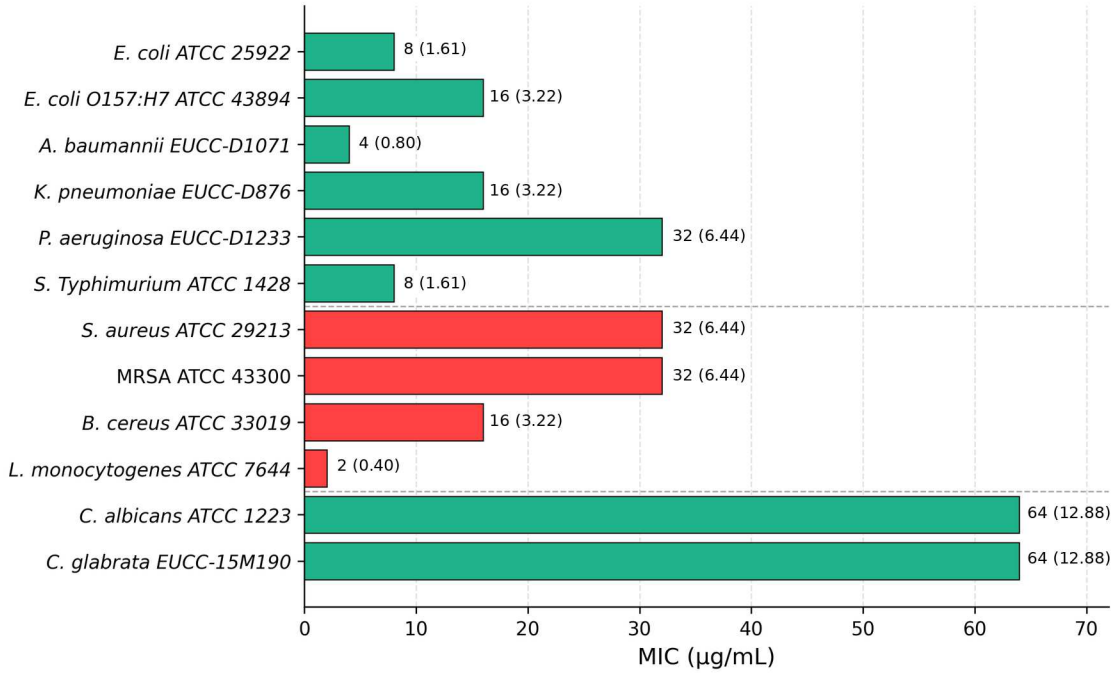


Construction and Molecular Verification of Recombinant *Pichia Pastoris* GS115/pPICZαA-385P

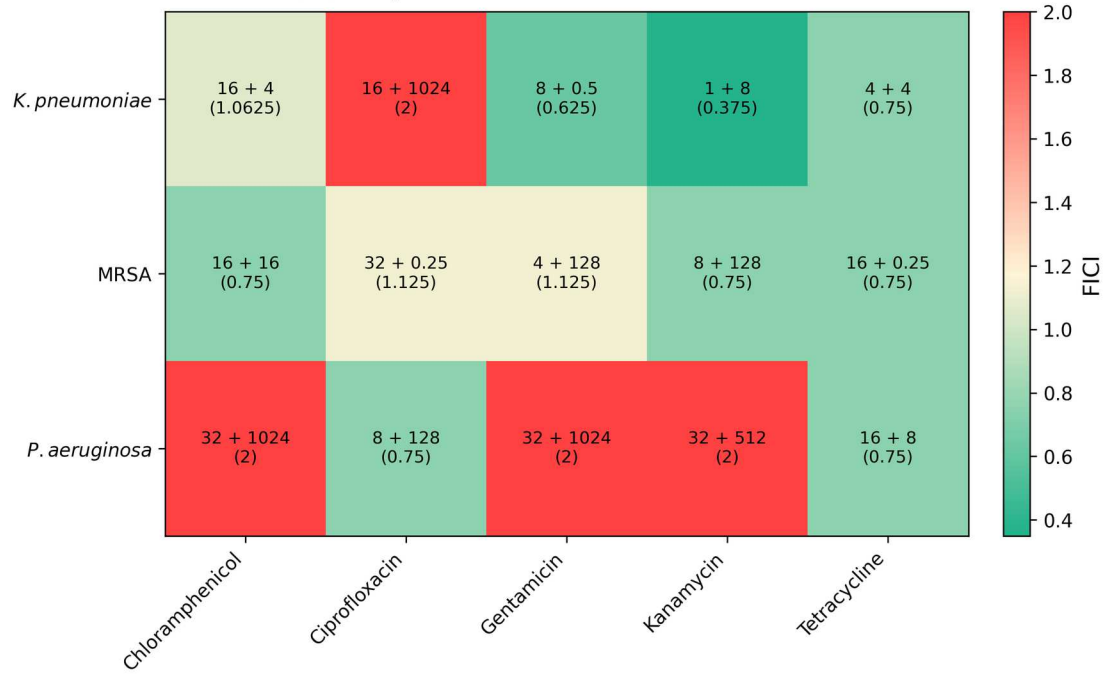



A
SDS–PAGE analysis
r385P
M
Marker
6 kDa
3 kDa
5 kDa
r385P
B
Western blot analysis
10 kDa
5 kDa
C
Structural analysis
CD spectrum
208 nm
222 nm
r385P
CD (mdeg)
Wavelength (nm)
BeStSel secondary structure composition (195–250 nm)
7.8%
8.0%
20.6%
63.6%
Disordered
β–Antiparallel
α–Helix
Turn
NRMSD = 0.03712 (195–250 nm)
D
Quantification with His–Tag ELISA
1 ng/mL
3 ng/mL
9 ng/mL
27 ng/mL
81 ng/mL
243 ng/mL
729 ng/mL
Standart curve
y = 2,0647x-0,589
R² = 0,9825
OD450nm
Standart Protein Concentration (ng/mL)

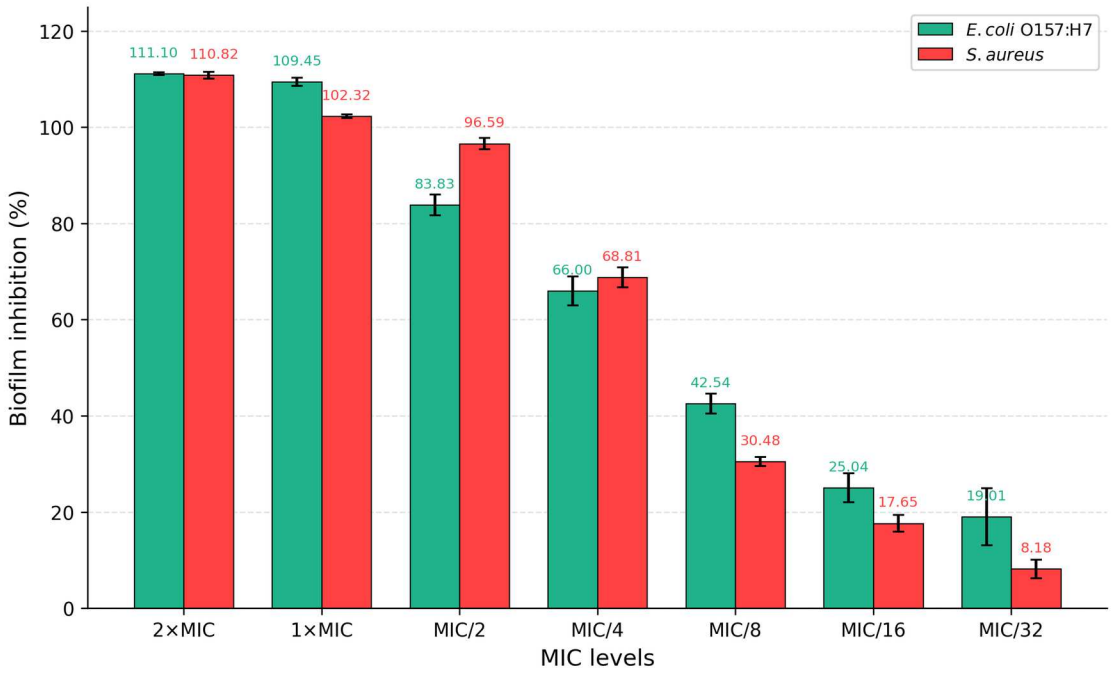
(A) Antimicrobial activity



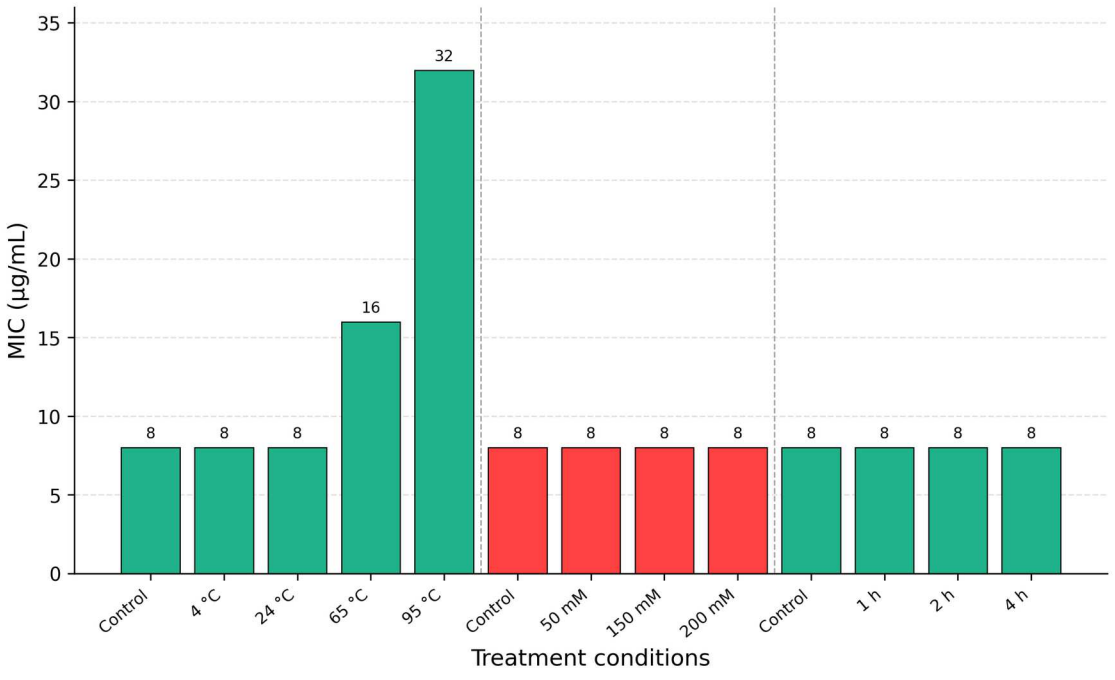
(B) Peptide–antibiotic interactions



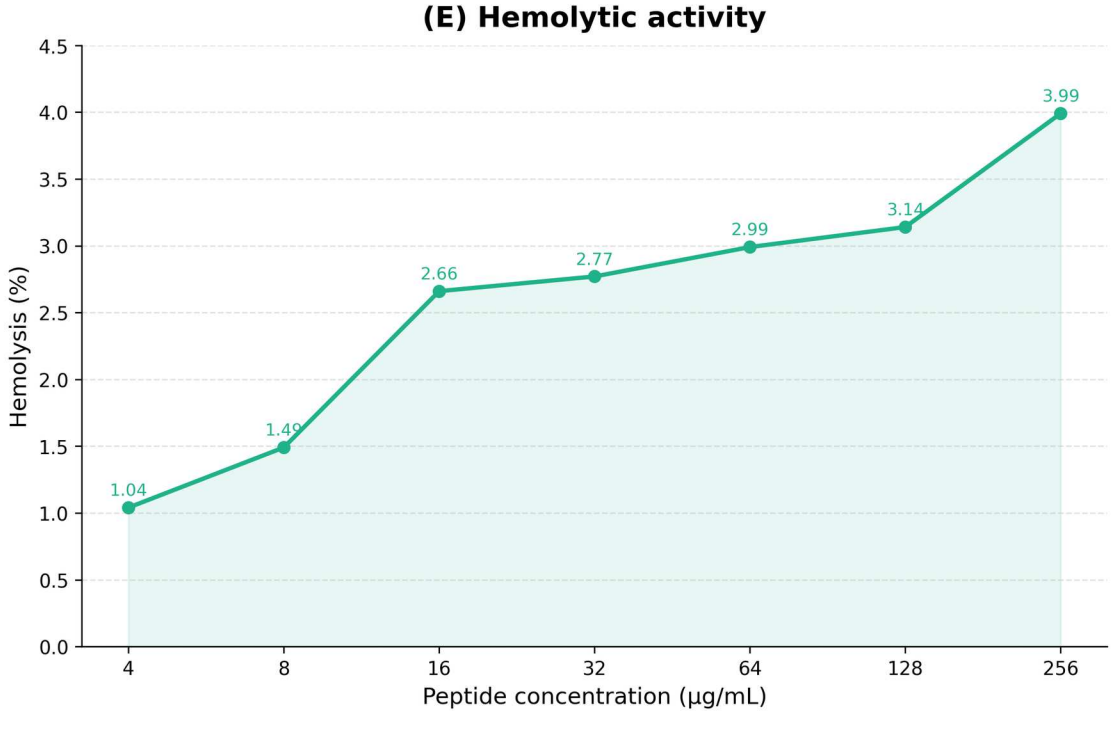
(C) Antibiofilm activity



(D) Stability



(E) Hemolytic activity



(F) MRC-5 cell viability

